Modelling and Control for a Rhombic-Like Vehicle: A case study

Chenshan Xu
chenshanxu@tecnico.ulisboa.pt

Instituto Superior Técnico, Universidade de Lisboa, Lisboa, Portugal

January 2021

Abstract

The work focuses on the design, validation, and comparison of different control solutions allowing a particular wheeled mobile robot - rhombic like vehicle to follow a reference path. The mathematical model of the rhombic like vehicle system (RLVs) consisting of a drive system, modules system, and the vehicle system is developed. Furthermore, the vehicle's kinematic model adherence to a nonholonomic constraint is studied for the control design purpose. A designing process of a controller based on the hierarchical approach is presented: i) low-level law for the motor speed control and ii) high-level control law for the vehicle position control. The low-level control for the motor system is based on the Proportional–Integral–Derivative(PID) control theory. The high-level control methodologies developed for position control are geometrical control and optimal control methods. A simulator is built in *Simulink/Matlab* to validate the designed controller.
Keywords: Wheeled mobile robot, Rhombic like vehicle, Nonholonomic constraints, Motion control, PID control, Linear control, Geometric control

1. Introduction

The research on the wheeled mobile robot (WMR) has been discussed in the past century. The interest of using wheeled mobile robot for several different applications is increasing worldwide nowadays [1], such as transportation in factories, warehouses, and places where there is a need for material delivery.
A particular rhombic like vehicle (RLV) with nonholonomic constraint is design for the transportation of equipment inside of the International thermonuclear experimental reactor (ITER). ITER project is one of the most aspiring energy projects today; it aims to explore nuclear fusion as a viable energy resource for the future. In order to achieve the ITER's main objective, the Remote Handling (RH) technique related with a transfer casks system was needed due to the restrictive presence of humans in inactivated areas during the maintenance operations. The main operation of RH equipment in ITER includes manipulating and exchanging components with weight up to 100 tons. A RLVs is particularly suitable for operations in the ITER cluttered environment (see Fig.1) because it enables higher maneuverability. It is type of vehicle equips with two drivable and steerable modules, the front and rear modules, each module with two wheels on the sides. The dissertation's theme is integrated into the FORMULAfusion project which aims to be a demonstration of a proof-of-concept with a scale robot of RLV with 250 kg of payload. Fig.2 showed

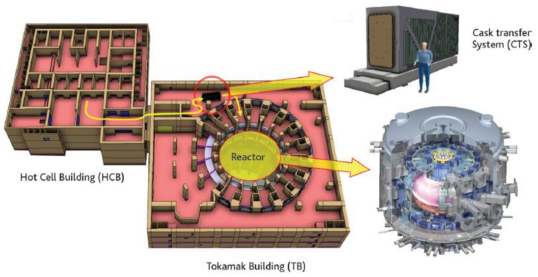

Figure 1: Simplified versions of two levels in the main buildings of ITER: storage and maintenance areas in the hot cell building (left) and divertor level of the tokamak reactor building (right) [2]

an automated vehicle with two steerable modules for cargo transportation using 3D CAD software.
There are three major challenges in the WMR autonomous navigation problem: localization[3, 4, 5], motion planning[2, 6, 7], and motion control[8, 9, 10, 11, 12]. This thesis studied the motion control problem, which the system receives as the input the motion plan in the previous stage - motion planning, and develop the feedback control law that allows the vehicle to track the desired trajectory. In order to reach this goal, the dissertation has two major objectives: the mathematical modeling of the RLVs scale prototype (see Fig.2), and developing the control solution for the vehicle motion control

problem. The work is organized as follows: Section 2 introduce the mathematical modeling of the RLVs model, developing the simulator; in Section 3 the proposed control solutions is presented; in Section 4 the results and final analysis of the thesis will be shown and Section 5 presents the conclusion and suggestions of future work to the proposed work.

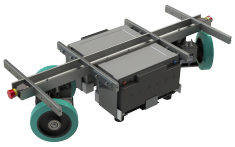

Figure 2: CAD representation of the RLVs without platform

The work presented in this thesis played an important contribution for the project FORMULAfusion of the Instituto de Plasmas Fusão Nuclear in Instituto Superior Técnico, University of Lisbon.

2. Mathematical Modelling

The RLVs planar representation is presented in Fig.3 to illustrate the main component of the system. The vehicle motion is defined with the body-fixed coordinate frame (x^B, y^B) and the fixed coordinate frame (X^I, Y^I). ψ is the projection of the angle from the X^B to the world's X^I and Y^I plane. It increases in the counter-clockwise direction, which implies that the vehicle's left turn signifies a positive radius. The vehicle pose is defined as (x, y, ψ), and it moves with linear speed v and angular speed ω of the vehicle until new definition is assigned. A

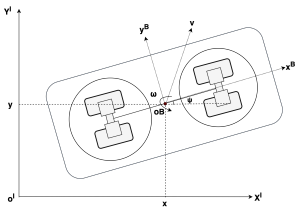

Figure 3: Vehicle coordinate system

formulation of the system aims to model the motion of the RLVs.

The approach is to separate the RLVs system into divided into three systems: drive system, modules system and vehicle system. In the following sections, each system will be described in detail.

2.1. Drive System Modeling

In this section, a modeling process of the drive system is developed. It is assumed that the vehicle is driven by four DC motors with mechanical gears. In Fig.4 a simplified scheme of the DC motor is depicted. The motor engine model used in the project

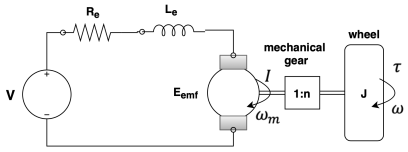

Figure 4: Decomposition of the system

FORMULAfusion is the MDXL61GN3IP, a single and integrated motor package (motor, drive and controller) sponsored by Applied Motion company (Reference: $J0200 - 408 - 4 - 000A$), as illustrated in Fig.5. According to the information provided by

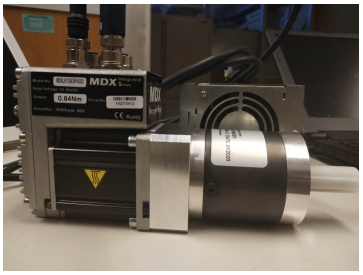

Figure 5: MDX Servo Motor

Applied Motion company, the motor specifications and parameters are given in Table 1. The dynamic

Table 1: Motor Model Parameter

Motor Parameters	**Value**
Armature Resistance	$R_e = 0.192\,\Omega$
Armature Inductance	$L_e = 0.56 \times 10^{-3}\,\mathrm{H}$
Torque constant	$K_t = 0.192\,\mathrm{N\,m\,A^{-1}}$
Voltage constant	$K_b = 0.392\,\mathrm{V/(rad/s)}$
Friction coefficient	$c = 3.0 \times 10^{-3}\,\mathrm{N\,m\,s^{-1}}$
Inertia	$J = 165 \times 10^{-7}\,\mathrm{kgm^2}$

equation of the motor is presented as follows:

$$\begin{aligned} R_e I + L_e \dot{I} + E_{emf} - V = 0 \\ J\dot{\omega}_m = \tau_m - c\omega_m \end{aligned} \tag{1}$$

where the torque generated by DC motor τ_m is proportional to the current, and the electromotive force E_{emf} proportional to the angular velocity as follows:

$$\begin{aligned} \tau_m = K_t I \\ E_{emf} = K_b \omega_m \end{aligned} \tag{2}$$

The whole gear system provides the gear ratio n, where $n = 84$, thus:

$$\begin{aligned} \tau &= nK_t I \\ \omega &= \frac{\omega_m}{n} \end{aligned} \tag{3}$$

with τ the torque acting on the wheels, and ω is denoted as the angular speed of the wheel until a new definition is assigned. Additional dynamic effects related to the mechanical gear system are herein not considered.

2.2. Modules System Modeling

After analyzing the drive system, one obtains the torque τ_{ij} and wheel angular speed ω_{ij} as the drive system's output. To understand how the wheel torque effect the vehicle's motion, the relation between the module velocity and orientation with the wheel angular speed is presented in this section.
As two modules have same configuration, the modeling of the module system is identical for the front and rear module. The first module is implemented in the scope of the project. Fig.6 shows a module with two parallel driven wheels, each wheel is attached with a drive system and a power supply. For the mathematical analysis of the module model,

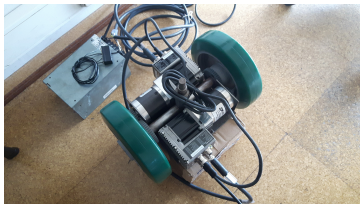

Figure 6: Module prototype attached with drive system

based on the Fig.6, the model representative of the module is presented in Fig.7. According to the geometric relations, the forward velocity v_x and angular rate $\dot{\theta}$ (denoted as ω in Fig.7) depends on both two wheels angular velocities as:

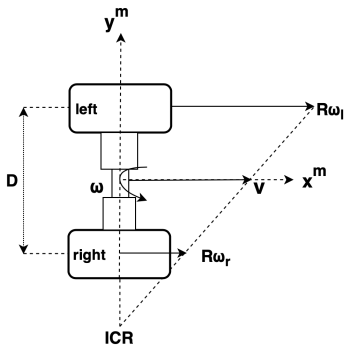

Figure 7: Model representative of the front module

$$\begin{aligned} v_x &= \frac{R\omega_r + R\omega_l}{2} \\ \omega &= \frac{R\omega_r - R\omega_l}{D} \end{aligned} \tag{4}$$

Therefore the modules linear and angular speed is now expressed in function of four wheel angular speed ω_{fr}, ω_{fl}, ω_{rr} and ω_{rl} as:

$$\begin{bmatrix} v_f \\ \dot{\theta}_f \\ v_r \\ \dot{\theta}_r \end{bmatrix} = \begin{bmatrix} \frac{R}{2} & \frac{R}{2} & 0 & 0 \\ \frac{R}{D} & -\frac{R}{D} & 0 & 0 \\ 0 & 0 & \frac{R}{2} & \frac{R}{2} \\ 0 & 0 & \frac{R}{D} & -\frac{R}{D} \end{bmatrix} \begin{bmatrix} \omega_{fr} \\ \omega_{fl} \\ \omega_{rr} \\ \omega_{rl} \end{bmatrix} \tag{5}$$

with D the distance between the wheels and R the wheel radius. The active force is generated by the motor which are aligned to the wheels. The force diagram with all active forces is presented in Fig.8. θ_f and θ_r are the modules orientations, and F_{ij} the

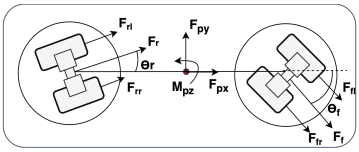

Figure 8: Force diagram for the vehicle

active forces of the vehicle with $i = (f, r)$ refer to the front, and rear modules and $j = (l, r)$ to the left and right wheels, respectively. The F_f and F_r are the resulting force acting on the front and rear module, respectively. F_{px} and F_{py} are the resulting forces in the x and y direction, and M_{pz} the moment, in the center of the vehicle.
The active force on the wheel can be calculated as:

$$F_{ij} = \frac{\tau_{ij}}{R} \tag{6}$$

with τ_{ij} the torque action on the wheels, and R the wheel radius.
The calculation of the resulting forces of the modules level in the vehicle frame is performed once each module's orientation is determined. For the analysis of the forces, the following relation is obtained according to Fig.8:

$$\begin{aligned} F_{ij_x} &= F_{ij} \cos\theta_i \\ F_{ij_y} &= F_{ij} \sin\theta_i \end{aligned} \tag{7}$$

with the index i refers to the i-th module, j refers to the j-th wheel.
The resulting forces in x and y direction, and moment from the action of the modules system are obtained in relation to the vehicle center of gravity's local coordinate system:

$$F_{px} = F_{f_x} + F_{r_x} = (F_{fr_x} + F_{fl_x}) + (F_{rr_x} + F_{rl_x}) \tag{8}$$

$$F_{py} = F_{f_y} + F_{r_y} = (F_{fr_y} + F_{fl_y}) + (F_{rr_y} + F_{rl_y}) \quad (9)$$

$$M_{pz} = \frac{D}{2}(F_{fr_x} + F_{rr_x}) - \frac{D}{2}(F_{fl_x} + F_{rl_x}) + L_f(F_{fr_y} + F_{fl_y}) - L_r(F_{rr_y} + F_{rl_y})) \quad (10)$$

from now on the ω is denoted as the angular speed of the vehicle. D the distance between the left and right wheels, L_f,L_r the distance of the front, rear module to the vehicle center of gravity, respectively.

2.3. Vehicle Motion

After analyzing the drive system and modules system, one obtains the active forces (F_{px}, F_{py}) and moments M_{pz} acting on the center of the vehicle. Additionally, the friction forces is considered and it is defined as a function of the vehicle's speed:

$$\begin{aligned} F_{ax} &= \mu_x v_x \\ F_{ay} &= \mu_y v_y \end{aligned} \quad (11)$$

where μ_x and μ_y are the friction coefficients. The value of the friction coefficients are related to the actual pose of the RLVs and the surface condition of the work environment. It can be obtained experimentally. Due to lack of the information, the first estimation of the friction value is made based on the [2], and then adjusted to the RLVs model in studied.

Thus the velocities of the vehicle in the body frame are presented as follows:

$$\dot{v}_x = \frac{1}{M}(F_{px} - \mu_x v_x - \omega M v_x) \quad (12)$$

$$\dot{v}_y = \frac{1}{M}(F_{py} - \mu_y v_y - \omega M v_y) \quad (13)$$

$$\dot{\omega} = \frac{1}{I_z} M_{pz} \quad (14)$$

where M is the mass of the vehicle, I_z the vehicle inertia. For control and navigation purposes, the velocity vector expressed in the vehicle frame (x^B, y^B) must be transformed to the global frame (X^I, Y^I), and this leads to the kinematics relations. Consider the coordinates (x, y, ψ) give the vehicle position in the global frame; it may be regarded as an integration of the inertial velocities v^I in the global frame with the following relations:

$$v^I = \begin{bmatrix} \dot{x} \\ \dot{y} \\ \dot{\psi} \end{bmatrix} = R_B^I \begin{bmatrix} v_x \\ v_y \\ \omega \end{bmatrix} \quad (15)$$

with

$$R_B^I = \begin{bmatrix} \cos\psi & -\sin\psi & 0 \\ \sin\psi & \cos\psi & 0 \\ 0 & 0 & 1 \end{bmatrix} \quad (16)$$

Based on the modeling equations of the previous sections, a simulator was built in *Matlab/Simulink* for the validation of the control system using the model parameters presented in Table 2.

Table 2: Vehicle Parameters Simulation setup

Vehicle parameters	**Value**
L_f	0.5 m
L_r	0.5 m
Vehicle width	0.7 m
Vehicle length	1.1 m
Distance between the wheels	0.25 m
Wheel radius	0.1 m
Vehicle Inertia	250 kgm^2
Total Mass of the Vehicle	375 kg
Maximum speed	$v = 0.5$m s^{-1}

3. Motion Control

The motion control is based on the schematic diagram of the control system as shown in Fig.9, where the system's global input is the reference position $(x_{ref}, y_{ref}, \psi_{ref})$, and suppose the current position (x, y, ψ) of the RLVs is measurable. The position control output is the four angular speed of the wheel. The control objective is to minimise the position and orientation errors $\tilde{q}$, and it is defined as follows:

$$\tilde{q} = q_{ref} - q = \begin{bmatrix} \tilde{q}_x & \tilde{q}_y & \tilde{q}_\psi \end{bmatrix} \quad (17)$$

In short, the motion control problem's solution is based on a hierarchical approach: i) low-level control law for the speed control of the drive system and ii) high-level control law for the position control.

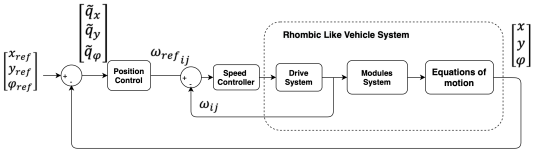

Figure 9: Schematic diagram of control system

3.1. Speed controller for the DC motor

For a motion control purpose, a speed controller based on the PID theory in the motor level is implemented to ensure the tracking features. In this case, the control law is defined as:

$$\frac{V_{ij}(s)}{E_{ij}(s)} = K_p + K_i \frac{1}{s} + K_d s \quad (18)$$

where the $E_{ij}(s)$ is the speed tracking error:

$$E_{ij}(s) = (\omega_{ref} - \omega)_{ij}$$

K_p is the proportional gain, K_i is the integral gain, and K_d is the derivative gain.

The transfer function of the DC motor is obtained

using the motor parameters in Table 1:

$$\frac{\omega_m(s)}{V(s)} = \frac{1}{1.42 \times 10^{-7}s^2 + 7.46 \times 10^{-5}s + 9.20 \times 10^{-3}} \tag{19}$$

The speed controller design via root locus method[13] is performed. Final PID parameters are presented in Table 3. The comparison between the

Table 3: PID Speed Controller Parameters

Controller Parameters	Value
K_p	50
K_i	5
K_d	0.5

simulation in *Simulink* and the experimental results in *MDX Servo Suite* is analyzed. Additional white noise was implemented to the motor model in order to get more realistic simulation results. The final result is presented in Fig.10.

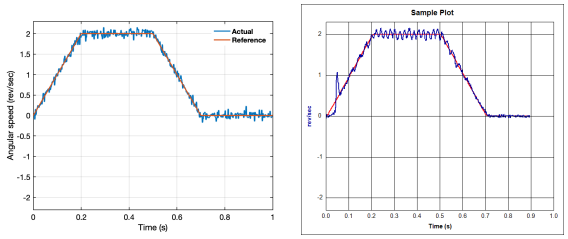

(a) *Simulink* (b) *MDX Servo Suite*

Figure 10: Comparison between the simulation and the experimental results

3.2. Alonzo Kelly Modified Controller

A kinematic model of RLVs based on a pure geometric study is presented in this section for control-oriented studies, and it is adherent to the nonholonomic constraints. Based on [14] the following equations are valid:

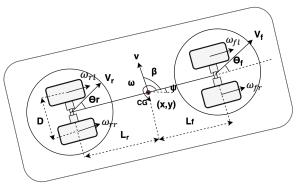

Figure 11: RLVs variables and parameters

$$\begin{bmatrix} \dot{x} \\ \dot{y} \\ \dot{\psi} \end{bmatrix} = \begin{bmatrix} \cos(\beta + \psi) \\ \sin(\beta + \psi) \\ \frac{(\tan\theta_f - \tan\theta_r)\cos\beta}{L_r + L_f} \end{bmatrix} v \tag{20}$$

where β is the slip angle of the vehicle.

$$\beta = \arctan\frac{L_r \tan\theta_f + L_f \tan\theta_r}{L_r + L_f} \tag{21}$$

$$v = \frac{v_f \cos\theta_f + v_r \cos\theta_r}{2\cos\beta} \tag{22}$$

The RLVs is considered as rigid body itself therefore the geometric constraints must be obeyed. The geometric constraint is expressed as follows:

$$v_f \cos\theta_f = v_r \cos\theta_r \tag{23}$$

According to Fig.11, to obtain the values of $(v_f, \theta_f, v_r, \theta_r)$, and meanwhile respecting the rigid body constraint (23), the following relations between the modules speed and vehicle speed must be verified:

$$\begin{bmatrix} v_{fx} \\ v_{fy} \\ v_{rx} \\ v_{ry} \end{bmatrix} = \begin{bmatrix} 1 & 0 & 0 \\ 0 & 1 & L_f \\ 1 & 0 & 0 \\ 0 & 1 & -L_r \end{bmatrix} \begin{bmatrix} v_x \\ v_y \\ \omega \end{bmatrix} \tag{24}$$

where

$$\begin{aligned} v_x &= v\cos\beta \\ v_y &= v\sin\beta \end{aligned} \tag{25}$$

and L_f, L_r are the distance of the front and rear module to the vehicle CG, respectively. The module orientation can be obtained using the trigonometric relation:

$$\theta_i = \arctan 2\frac{v_{iy}}{v_{ix}} \tag{26}$$

and the linear velocity of the module:

$$v_i = \sqrt{{v_{ix}}^2 + {v_{iy}}^2} \tag{27}$$

The module is equipped with two wheels, and each wheel is attached with a motor. In body frame, the angular velocities of the wheels can be obtained from the modules speed as:

$$\begin{bmatrix} \omega_{fr} \\ \omega_{fl} \\ \omega_{rr} \\ \omega_{rl} \end{bmatrix} = \frac{1}{R}\begin{bmatrix} 1 & \frac{D}{2} & 0 & 0 \\ 1 & -\frac{D}{2} & 0 & 0 \\ 0 & 0 & 1 & \frac{D}{2} \\ 0 & 0 & 1 & -\frac{D}{2} \end{bmatrix} \begin{bmatrix} v_f \\ \dot{\theta}_f \\ v_r \\ \dot{\theta}_r \end{bmatrix} \tag{28}$$

with R the wheel radius, and D the distance between two wheels. Hence, this transformation allows that motion control thought $[v, \beta, \omega]$, inside of $[\omega_{fr}, \omega_{fl}, \omega_{rr}, \omega_{rl}]$.

Two feedback control laws are here introduced based on the principle presented in [15, 16, 17], and extended to the RLVs in studied. The main idea of the methodology is to control the RLVs motion thought the control of $[v^c, \beta^c, \omega^c]$ (see Fig.12). The output would be the angular velocities of the wheel:

$[\omega^c_{fr}, \omega^c_{fl}, \omega^c_{rr}, \omega^c_{rl}]$ that enable the RLVs follow the desired path. For the control law design, the v^c is assumed to be predefined and the speed information is contained in the reference trajectory. The control variable β^c is obtained using the geometric law as presented in Fig.12, and it is used to direct the vehicle's to the reference pose. As for control variable ω^c, it aims to orientating RLVs to the desired orientation. The control law for those two variables is

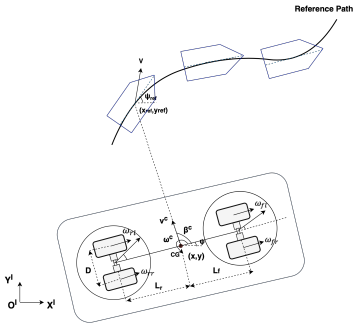

Figure 12: Alonzo Kelly Modified controller representation and variables definition

presented as follows:

$$\beta^c = \arctan \frac{x_{ref} - x}{y_{ref} - y} - \psi$$
$$\omega^c = \frac{k_\omega(\psi_{ref} - \psi)}{t_n} \tag{29}$$

where the $(x_{ref}, y_{ref}, \psi_{ref})$ are the coordinate of reference path pose and (x, y, ψ) the actual coordinate of RLVs. t_n the simulation step and k_ω a positive gain that tunes the RLVs to desired orientation. In brief, the AKM controller works as a proportional controller, where the control variables are proportional to the heading angle error and the cross track errors.

For the path following task simulation, as the RLVs will be operating the ITER with the cluttered work environment, in order to simulate the work conditions, the direction path is designed. The simulation result in the kinematic model (20) is presented in Fig.13. One drawback of this method is the oscillation in the requested wheel speed (see Fig.13(d)) which may cause damage to the system actuator. The simulation with the kinematic model was able to capture the essential characteristics of the AKM controller. However, a more precise simulation is done with the RLVs simulator presented section 2. Table 4 summarizes the controller performance with the given reference in both two models with the position errors (δ_x, δ_y) and orientation errors δ_ψ. The simulation in the RLVs simulator is worst because the dynamic effects are not considered at the controller design stage. The oscillation of the position error in Fig.13(b) is mainly caused by introducing

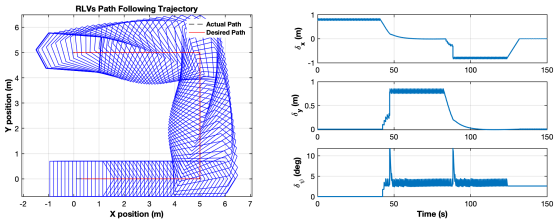

(a) Resulting trajectory (b) Errors

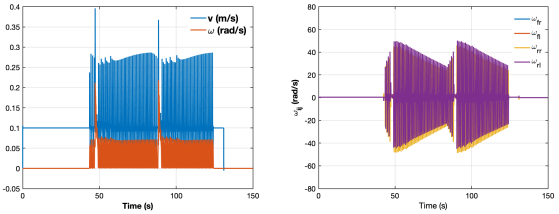

(c) Resulting vehicle speed (d) Resulting wheel speed

Figure 13: AKM controller: simulation in the kinematic model

Table 4: Simulation result (root mean square (RMS) values of selected variables)

AKM controller	$\delta_x(m)$	$\delta_y(m)$	$\delta_\psi(deg)$
Kinematic model	0.59	0.40	2.79
RLVs simulator	0.87	0.68	6.63

the look-ahead distance. The position error can be decreased if the smaller value of look-ahead distance is used. Table 5 demonstrates the position error decreased with the decrease of the look ahead distance. However, a smaller look ahead distance can cause strong oscillations, and the system became challenging to stabilize.

Table 5: Influence of the look ahead distance

look ahead distance	$\delta_x(m)$	$\delta_y(m)$	$\delta_\psi(deg)$
0.2	0.15	0.10	2.58
0.5	0.38	0.26	2.67
0.8	0.87	0.68	6.63

3.3. Linear Quadratic Regulator

A LQR optimal control for trajectory tracking of RLVs is developed in this section, which calculates optimally the necessary linear and angular velocity to follow a reference signal. Consider the optimal regulator problem that, given the system equation:

$$\dot{x} = Ax + Bu$$

determines the matrix K of the optimal control vector

$$u = -Kx$$

so as to minimize a certain cost function. For the infinite horizon problem, the cost function and conditions is defined as:

$$\begin{aligned} J^* = min_u \int_0^\infty (x(t)^T Q x(t) + u(t)^T R u(t)) dt \\ \dot{x}(t) = Ax(t) + Bu(t) \\ x(0) = x_0 \end{aligned} \tag{30}$$

The system is consider in the steady state condition, therefore the solution can be considered as an ARE (Algebraic Riccati Equation):

$$A^T P_{ss} + P_{ss} A - P_{ss} B R^{-1} B^T P_{ss} + Q = 0 \tag{31}$$

and

$$u_{opt}(t) = -Kx(t) \tag{32}$$

with

$$K(t) = -R^{-1} B^T P_{ss}$$

For the trajectory tracking problem, given a system $\dot{x} = f(x, u)$ and a reference trajectory (x_{ref}, y_{ref}), the problem becomes to calculate a compensator of the form $u = K(x, x_{ref}, u_{ref})$ such that when t goes to infinity, the position error is equals to zero.
The error in the inertial frame $\dot{\tilde{q}}_I = (\tilde{q}_x, \tilde{q}_y, \tilde{q}_\psi)_I$ are:

$$\begin{bmatrix} \tilde{q}_x \\ \tilde{q}_y \\ \tilde{q}_\psi \end{bmatrix}_I = \begin{bmatrix} \cos\psi & \sin\psi & 0 \\ -\sin\psi & \cos\psi & 0 \\ 0 & 0 & 1 \end{bmatrix} \begin{bmatrix} q_x \\ q_y \\ q_\psi \end{bmatrix}_B \tag{33}$$

For the control design purpose, the result of tangent linearization of system about the reference trajectory in the global frame is presented:

$$\dot{\tilde{q}}_I = \begin{bmatrix} 0 & \omega_{ref} & 0 \\ -\omega_{ref} & 0 & v_{ref} \\ 0 & 0 & 0 \end{bmatrix} \tilde{q}_I + \begin{bmatrix} 1 & 0 \\ 0 & 0 \\ 0 & 1 \end{bmatrix} \begin{bmatrix} \tilde{v} \\ \tilde{\omega} \end{bmatrix} \tag{34}$$

For the reference trajectory defined as $(x_{ref}, y_{ref}, \psi_{ref})$, the v_{ref} and ω_{ref} can be calculated from following equations according to [12]:

$$\psi_{ref} = \arctan \frac{\dot{y}_{ref}}{\dot{x}_{ref}} \tag{35}$$

having differentiation of (35) in order to get ω_{ref} as:

$$\omega_{ref} = \frac{\dot{x}_{ref} \ddot{y}_{ref} - \dot{y}_{ref} \ddot{x}_{ref}}{\dot{x}_{ref}^2 + \dot{y}_{ref}^2} \tag{36}$$

$$v_{ref} = \pm \sqrt{\dot{x}_{ref}^2 + \dot{y}_{ref}^2} \tag{37}$$

The sign for v_{ref} will define forward or backward motion of vehicle. The desired cartesian motion reference (x_{ref}, y_{ref}) should be twice differential according to the (36).

The system (34) has three state variables $[\tilde{q}_x, \tilde{q}_y, \tilde{q}_\psi]$, representing the dynamics of tracking error in coordinate (x, y, ψ), and two inputs $[\tilde{v}, \tilde{\omega}]$. In order to determine inputs of the closed-loop system the LQR optimal control is used. According to the LQR control theory, the solution can be obtained as

$$u_{opt}(t) = -K\tilde{x}(t)$$

where K is the gain matrix determined by LQR controller optimally. The Bryson method is used for the first estimation of the weighting matrices of the states and inputs, respectively Q and R, as diagonal matrices where each term is the inverse square of the expected maximum for the variable during the motion:

$$\begin{aligned} Q &= diag(Q_i) \\ Q_i &= \frac{1}{q_{i,max}^2} \end{aligned} \tag{38}$$

with $q_{i,max}$ maximum acceptable value of q_i in SI unit. According to the ITER project specification, the vehicle has to move in cluttered environments with safety margins of 30 cm, therefore the maximum accepted value for the $\tilde{q}_x$ and $\tilde{q}_y$ are approximately 0.3 m, and 0.15 radius for the vehicle orientation. The final value is presented below based on the (38):

$$Q(\tilde{q}_x, \tilde{q}_y, \tilde{q}_\psi) = diag(10, 10, 50) \tag{39}$$

Same principle is used for the matrix R:

$$\begin{aligned} R &= diag(R_i) \\ R_i &= \frac{1}{u_{i,max}^2} \end{aligned} \tag{40}$$

with $u_{i,max}$ max acceptable value of u_i.

$$R(\tilde{v}_{ref}, \tilde{q}_{ref}) = diag(5, 1) \tag{41}$$

By changing the elements of Q, the sensitivity of the system to the state variables can be adjusted. Therefore, to obtain the inputs of the system, the Equation (42) is available:

$$\begin{bmatrix} v^c \\ \omega^c \end{bmatrix} = -K \begin{bmatrix} \tilde{q}_x \\ \tilde{q}_y \\ \tilde{q}_\psi \end{bmatrix}_I \tag{42}$$

with K the gain matrix determined by LQR controller optimally and the system is extended with determination of β^c(29).
A pose tracking problem is studied to investigate the stabilization feature of the LQR controller, and the relation between the module's orientation and the vehicle heading angle is also discussed. The desired pose is position $(5, 5)$m with zero heading angle. The chosen initial conditions for the RLVs

is $(0, 0)$m with zero heading angle. This case study aims to illustrate how the vehicle can slide to the desired position without changing the vehicle heading angle. The study of how the model parame-

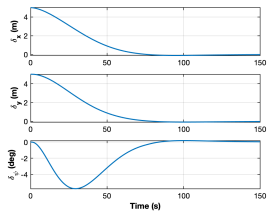

(a) Resulting errors

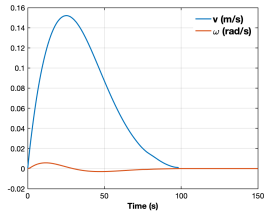

(b) Resulting linear and angular speed

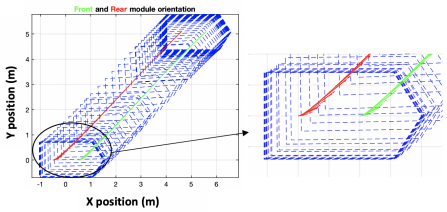

(c) Resulting modules orientation: the green arrow represents the front module and the red arrow represents the rear module

Figure 14: LQR controller: initial conditions $(x, y, \psi) = (0, 0, 0)$; desired pose: $(5, 5, 0)$

ters' variation, in this case, a wheel radius and vehicle mass, effects on the controller performance is presented. The simulation's case mission is considered a circle path with null initial conditions. According to (37) and (36), the reference velocities are calculated, where the $v_{ref} = 0.2\,\mathrm{m\,s^{-1}}$ and $\omega_{ref} = 0.05\,\mathrm{rad\,s^{-1}}$ clockwise.
Fig.15(a) is the resulting trajectory of the vehicle, and the vehicle follows the reference trajectory with the minimum position error. The resulting vehicle velocities are presented in Fig.15(b), where the linear speed v oscillated around the v_{ref} and angular speed approximated to the ω_{ref}. Several sim-

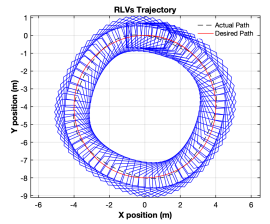

(a) Resulting trajectory

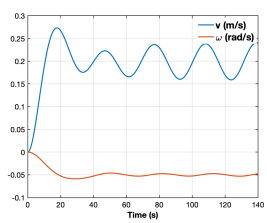

(b) Resulting linear and angular speed

Figure 15: Baseline simulation for the study of the robustness of the LQR controller

ulations are done with the variation of the vehicle mass and wheel radius. Fig.16(a) showed the position and orientation errors increase with the increase of the vehicle mass. This is due to the fact of the controller is designed based on the kinematic model. As the mass increases, the vehicle's inertial effect becomes significant, and the system can not respond to the request control action as quickly as it is supposed to be, which causes the controller performance to become worse. Fig.16(b) showed the variation of the wheel radius effects more in the position x and y than the vehicle orientation. This kind of mismatch in the wheel radius in reality can be caused by various reasons, such as tire wear or measurement errors. The tire's wear can be a severe problem, and depends on the type of tire will be used, the scale of variation can be considerable. However, as the wheel radius parameter is a measurable variable, and generally speaking, for a large and heavy-duty vehicle, the maximum tire wear permitted is around $60mm$[1], including the eventual measurement error, the LQR is considered to be robust to 50% variation of the wheel radius parameter.

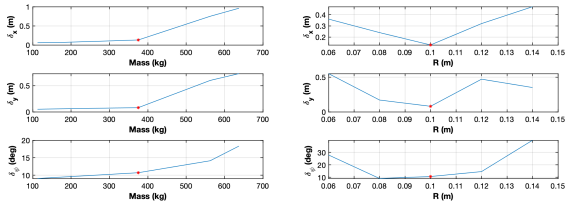

(a) Influence of M

(b) Influence of R

Figure 16: Study of the robustness: red mark represents the baseline simulation

4. Results

Two types of control solutions described in the previous sections present their advantages and disadvantages. An overall comparison between them is crucial to provide a better overview of the different control options. In this section, this assessment is made considering parameters such as path-tracking performance for the several challenge paths (see Section 4.1), a case study mission which intent to evaluate the control effort of two controllers is presented in Section 4.2.

4.1. Performance for case-study mission

For the tracking error assessment, the cross-track error of the center of the RLVs, denoted by e_c, is used, and it is calculated as:

$$e_c = \sqrt{\delta_x^2 + \delta_y^2} \tag{43}$$

[1]Information provided by Technical Engineer in CRRC Tangshan Co., Ltd., a manufacturer of rolling stock located in Tangshan, Hebei province,China

where the δ_x and δ_y are the position error of the center of vehicle in x and y direction, respectively. The results show for all the path-tracking case in study, the LQR was able to follow the reference with less errors than AKM controller. However, the performance of two controllers relied a lot on the tuning parameters, and as the tuning process of the AKM controller is done empirically, a more precise study is presented in the next section to evaluate the difference between the two controllers for a case study mission.

Path	**Controller**	$e_c(m)$
Spiral	AKM	0.45
	LQR	0.36
Circle	AKM	0.43
	LQR	0.15
Direction Path	AKM	0.92
	LQR	0.40

Table 6: RMS of e_c for each of the controllers

4.2. Comparison of controller performance: case study

The mission case is defined as:

$$\begin{aligned} x_{ref} &= 0.1t \\ y_{ref} &= 0 \\ \psi_{ref} &= 0 \end{aligned} \tag{44}$$

and vehicle initial conditions are $(-2, -2)$m with zero heading angle.

The vehicle with LQR controller was able to enter the reference trajectory quicker than vehicle with AKM controller (see Fig.17). However after the entrance to the reference trajectory, the AKM controller presents less static errors than the LQR controller. For better validation of two controller, the RMS of errors is calculated and summarized in Table 7. Fig.18 show the requested torque of four motors for both two controllers. The value of torque is much smaller in the LQR controller, as the principle of the LQR is calculate the optimal control input

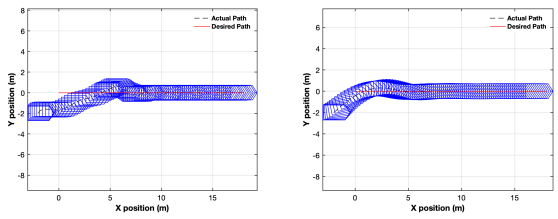

(a) AKM controller (b) LQR controller

Figure 17: Comparison of two controllers: resulting trajectories

Table 7: Comparison between two controllers (RMS values of selected variables)

Type of controller	$\delta_x(m)$	$\delta_y(m)$	$\delta_\psi(deg)$
LQR	1.16	0.49	5.95
AKM	0.87	0.69	0.01

that minimized the defined cost function. In order

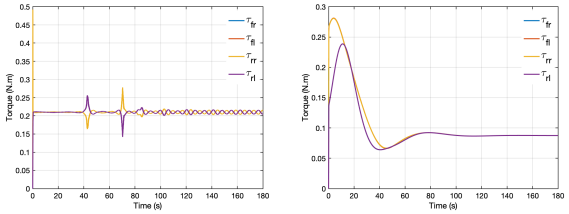

(a) AKM controller (b) LQR controller

Figure 18: Comparison of two controllers: actuators request

to better visualize of the relative results, Table 8 presents a qualitative overall comparison between controllers. The evaluation of the design parameters tuning provides a comparative idea of the necessary effort of the designer to correctly tune the controllers parameters. This evaluation is merely based on the knowledge acquired throughout this work, and serves only as an indication of the future work.

Table 8: Overall comparison between two controllers: (++ good, + average, – poor)

Type of controller	AKM	LQR
Tracking errors	++	+
Requested control effort	–	++
Code simplicity	++	+
Design parameters tuning	–	+

5. Conclusions

A mathematical model of RLVs is presented based on the dynamic and kinematic equations. A simulator is built in *Simulink* to validate the designed controller. Two controllers are proposed allowing the vehicle to follow a reference path. The validation of the two solutions for different tasks is performed. The simulation results show the performance of the AKM controller depends a lot on the tuning parameter. The advantages of the AKM controller are the design simplicity and the main disadvantage is the time-consuming tuning of the control design param-

eters. An LQR controller is designed for the position control based on the kinematic model. It still takes some time-consuming tuning of the control design parameters, namely the state and input control matrices. However, this time compared with the AKM controller is insignificant.
Both two control solutions, AKM and LQR controller, proved to be capable of executing different missions. An assessment of each controller's advantages and disadvantages and a comparison between them was also made, providing a comprehensive insight into the RLVs autonomous navigation control problem and the solutions proposed. During the development of this work, given the time limitations for this thesis development, some subject have not been addressed: development of the mathematical model of the RLVs including tire model and design of the controller with the dynamic vehicle effects and it would be also interesting to performed control design in discrete time and analyse the differences with the continuous case.

Acknowledgements
My appreciation goes to my supervisors, Doctor Alberto Vale and Professor Alexandra Moutinho for always been there listening even during the most challenging time of Covid-19.

References

[1] F. Rubio, F. Valero, and C. Llopis-Albert, "A review of mobile robots: Concepts, methods, theoretical framework, and applications," *International Journal of Advanced Robotic Systems*, vol. 16, no. 2, pp. 1–22, 2019.

[2] D. Fonte, *Motion Planning for a Rhombic-Like Vehicle Operating in ITER Scenarios*. PhD thesis, Instituto Superior Técnico, University of Lisbon, 2011.

[3] G. Li, D. Qin, and H. Ju, "Localization of Wheeled Mobile Robot Based on Extended Kalman Filtering," *MATEC Web of Conferences*, vol. 22, pp. 1–5, 2015.

[4] P. Goel, S. I. Roumeliotis, and G. S. Sukhatme, "Robust localization using relative and absolute position estimates," *IEEE International Conference on Intelligent Robots and Systems*, vol. 2, pp. 1134–1140, 1999.

[5] M. Doumbia and X. Cheng, "State estimation and localization based on sensor fusion for autonomous robots in indoor environment," *Computers*, vol. 9, no. 4, pp. 1–15, 2020.

[6] D. Glavaški, M. Volf, and M. Bonkovic, "Robot motion planning using exact cell decomposition and potential field methods," in *Proceedings of the 9th WSEAS international conference on Simulation, modelling and optimization*, pp. 126–131, World Scientific and Engineering Academy and Society (WSEAS), 2009.

[7] G. Dudek and M. Jenkin, *Computational Principles of Mobile Robotics*. Cambridge University Press, 2 ed., 2010.

[8] O. Amidi and C. Thorpe, "Integrated mobile robot control," *Fibers' 91, Boston, MA*, vol. 1388, no. May, pp. 504–523, 1991.

[9] S. F. Campbell, *Steering control of an autonomous ground vehicle with application to the DARPA urban challenge*. PhD thesis, Massachusetts Institute of Technology, 2007.

[10] S. Morales, J. Magallanes, C. Delgado, and R. Canahuire, "LQR Trajectory Tracking Control of an Omnidirectional Wheeled Mobile Robot," *2018 IEEE 2nd Colombian Conference on Robotics and Automation, CCRA 2018*, 2018.

[11] F. Lin, Z. Lin, and X. Qiu, "LQR controller for car-like robot," *Chinese Control Conference, CCC*, vol. 2016-Augus, pp. 2515–2518, 2016.

[12] A. Abbasi and A. J. Moshayedi, "Trajectory tracking of two-wheeled mobile robots, using lqr optimal control method, based on computational model of khepera iv," *Journal of Simulation and Analysis of Novel Technologies in Mechanical Engineering*, vol. 10, no. 3, pp. 41–50, 2018.

[13] N. Nise, M. Perez, A. Perez, E. Perez, N. Nise, S. Simrock, N. Siddique, and A. Carrillo, *Control Systems Engineering*, vol. 517. 2011.

[14] R. Solea, A. Filipescu, S. Filipescu, and B. Dumitrascu, "Sliding-mode controller for four-wheel-steering vehicle: Trajectory-tracking problem," in *2010 8th World Congress on Intelligent Control and Automation*, pp. 1185–1190, IEEE, 2010.

[15] R. C. Coulter, "Implementation of the Pure Pursuit Path Tracking Algorithm," Tech. Rep. January, The Robotics Institute Camegie Mellon University, Pittsburgh, Pennsylvania, 1992.

[16] A. Kelly and N. Seegmiller, "A vector algebra formulation of mobile robot velocity kinematics," in *Field and Service Robotics*, pp. 613–627, Springer, 2014.

[17] N. Silva, L. Baglivo, A. Vale, and M. D. Cecco, "Four Path Following Controllers for Rhombic Like Vehicles," *2013 IEEE International Conference on Robotics and Automation*, pp. 3204–3211, 2013.